

Supplementary information

Flagellar Motor Protein-Targeted Search for the Druggable Site of *Helicobacter pylori*

Vaishnavi Tammara^{a,b}, Ruchika Angrover^c, Disha Sirur^d, and Atanu Das^{a,b,*}

^aPhysical and Materials Chemistry Division, CSIR-National Chemical Laboratory, Dr. Homi Bhabha Road, Pune, Maharashtra 411008, India.

^bAcademy of Scientific and Innovative Research (AcSIR), Ghaziabad 201002, India.

^cThe Departments of the University Institute of Biotechnology, Chandigarh University, NH-05, Ludhiana – Chandigarh State Highway, Punjab 140413.

^dSchool of Physical Sciences, National Institute of Science Education & Research-Bhubaneswar, An OCC of Homi Bhabha National Institute, P.O. Jatni, Khurda, Odisha 752050, India.

*E-mail: as.das@ncl.res.in

This file contains the following information:

Figures S1 to S12

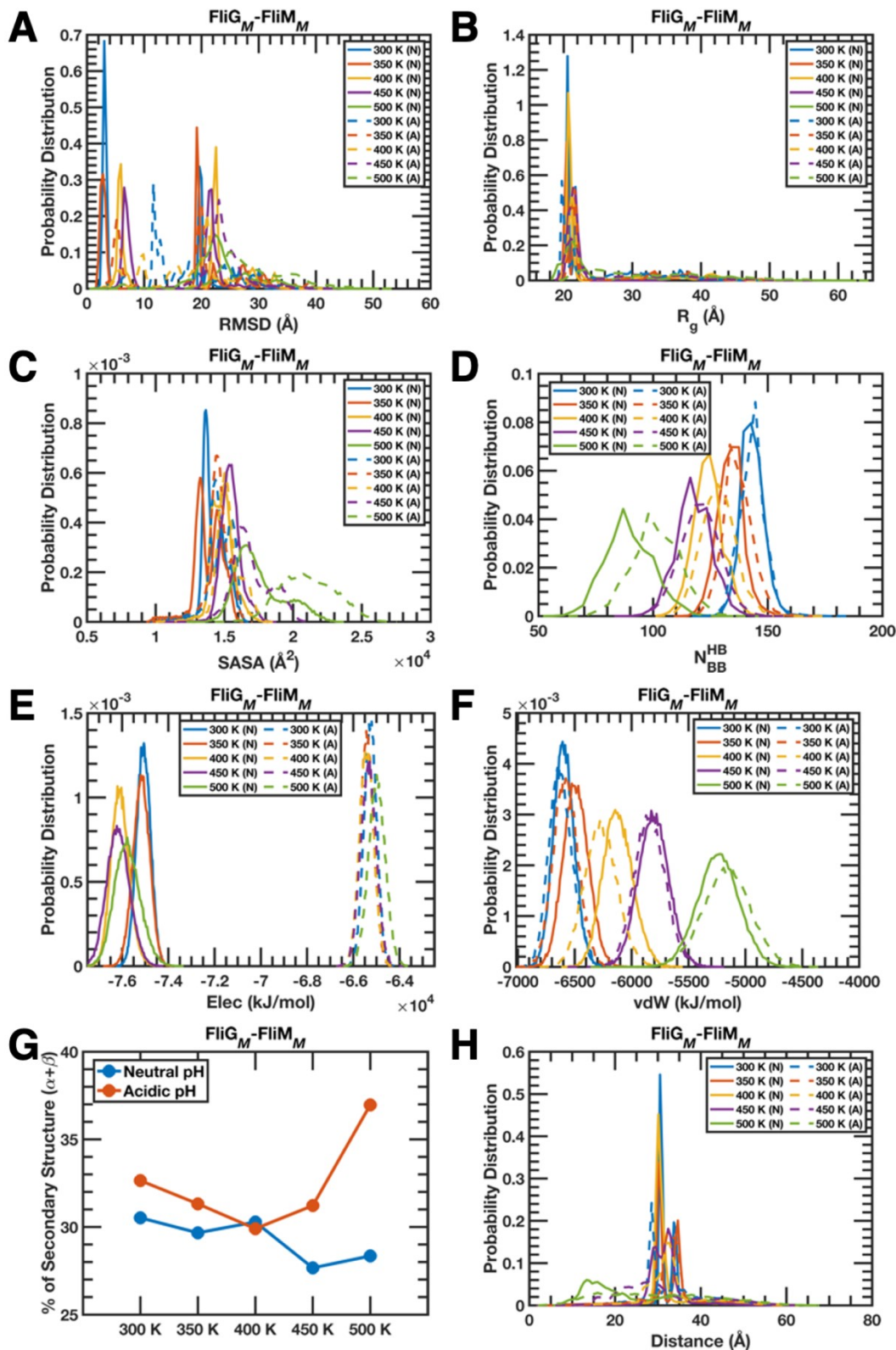


Figure S1. Structural and energetic properties of the $FliG_M-FliM_M$ complex evolved in the thermal scanning simulations in two pH conditions. Normalized probability distributions of – (A) backbone RMSD, (B) backbone C_α -based R_g , (C) global SASA, (D) backbone hydrogen bonds, (E) electrostatic interactions, and (F) van der Waal’s forces. (G) Variability in secondary structural features. (H) Normalized probability distributions of the distance between two protein sequences of the complex.

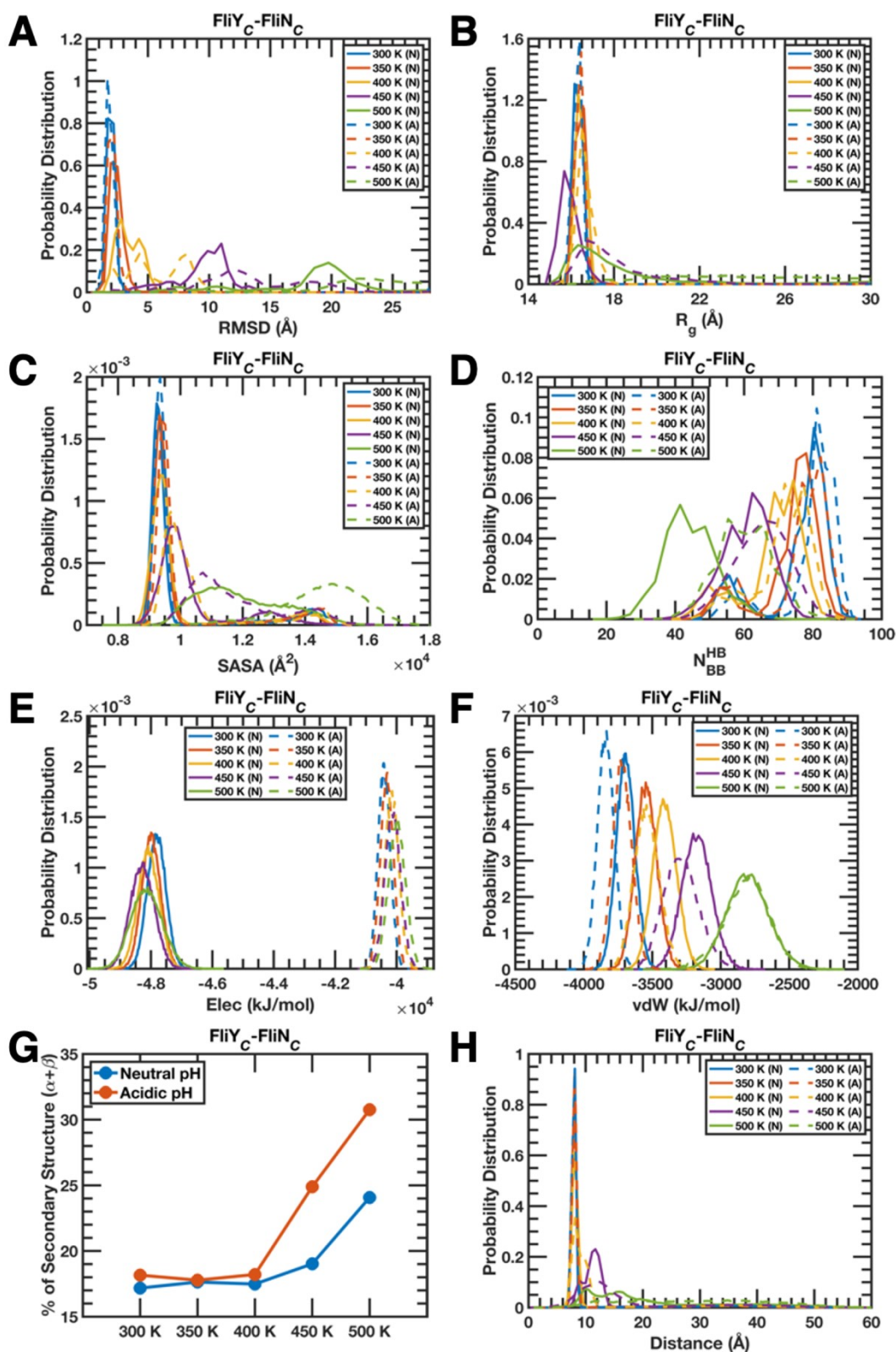


Figure S2. Thermal scanning-derived structural and energetic features of the FliY_C-FliN_C complex in neutral and acidic pH conditions. Normalized probability distributions of – (A) backbone RMSD, (B) backbone C_α-based R_g, (C) global SASA, (D) backbone hydrogen bonds, (E) electrostatic interactions, and (F) van der Waal's forces. (G) Secondary structural content in terms of α-helix and β-strand. (H) Normalized probability distributions of the distance between two complex-forming proteins.

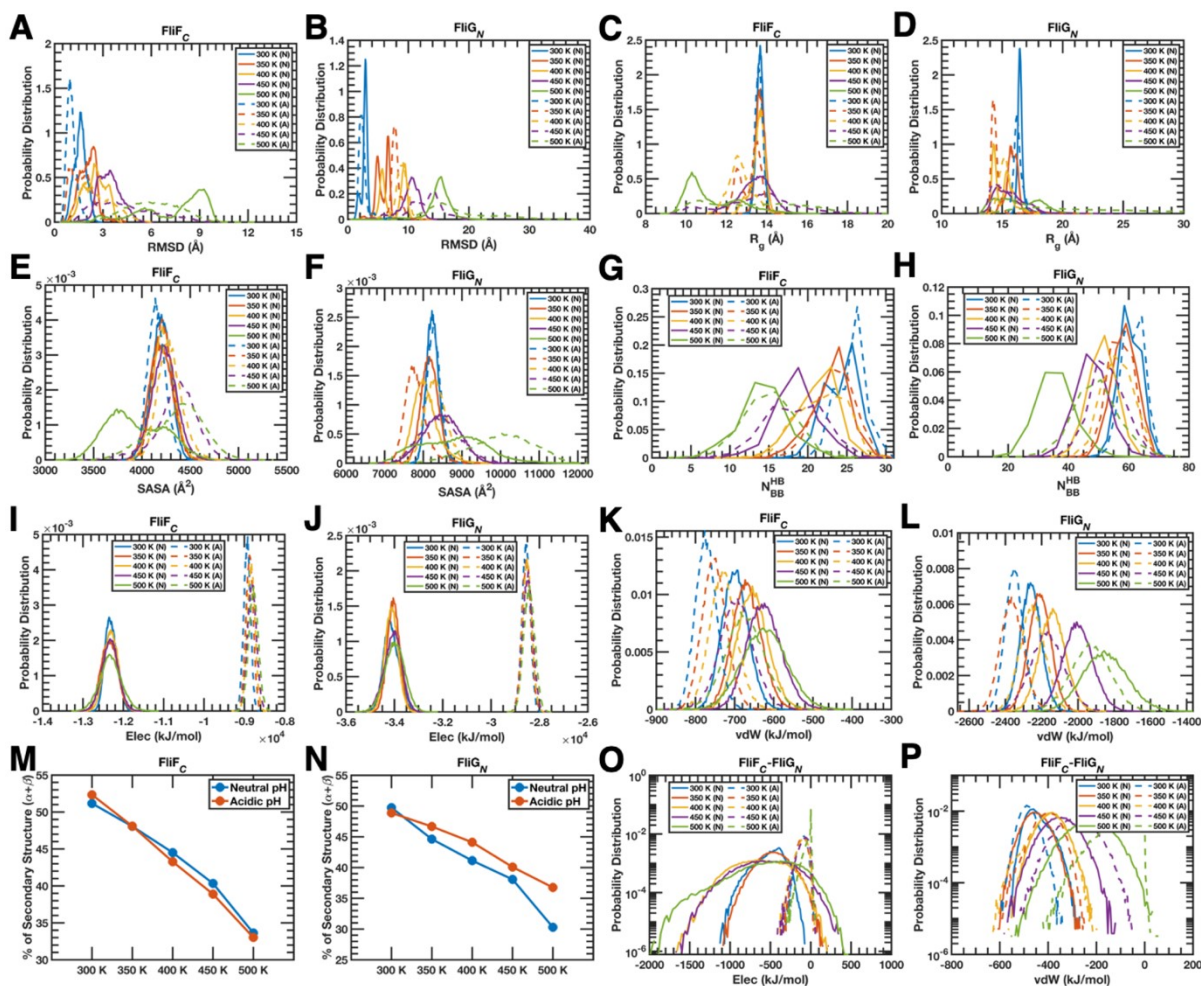


Figure S3. Evolution of structural and energetic features of the FliF_C and the FliG_N chains of the FliF_C-FliG_N complex at five different temperatures and in two different pH conditions. (A-L) Normalized probability distributions of the intra-protein characteristics – backbone RMSD of (A) FliF_C chain and (B) FliG_N chain; backbone C_α-based R_g of (C) FliF_C chain and (D) FliG_N chain; global SASA of (E) FliF_C chain and (F) FliG_N chain; backbone hydrogen bonds of (G) FliF_C chain and (H) FliG_N chain; electrostatic interactions of (I) FliF_C chain and (J) FliG_N chain; and van der Waal's forces of (K) FliF_C chain and (L) FliG_N chain. Temperature-dependence of the percentage of secondary structural content in terms of α -helix and β -sheet at two different pH of the solution of (M) FliF_C chain and (N) FliG_N chain. Normalized probability distributions of the variable inter-chain properties operative under dynamic solution conditions dictated by changing temperature and pH – (O) electrostatic forces operative between two chains and (P) dispersion interactions acting between two proteins.

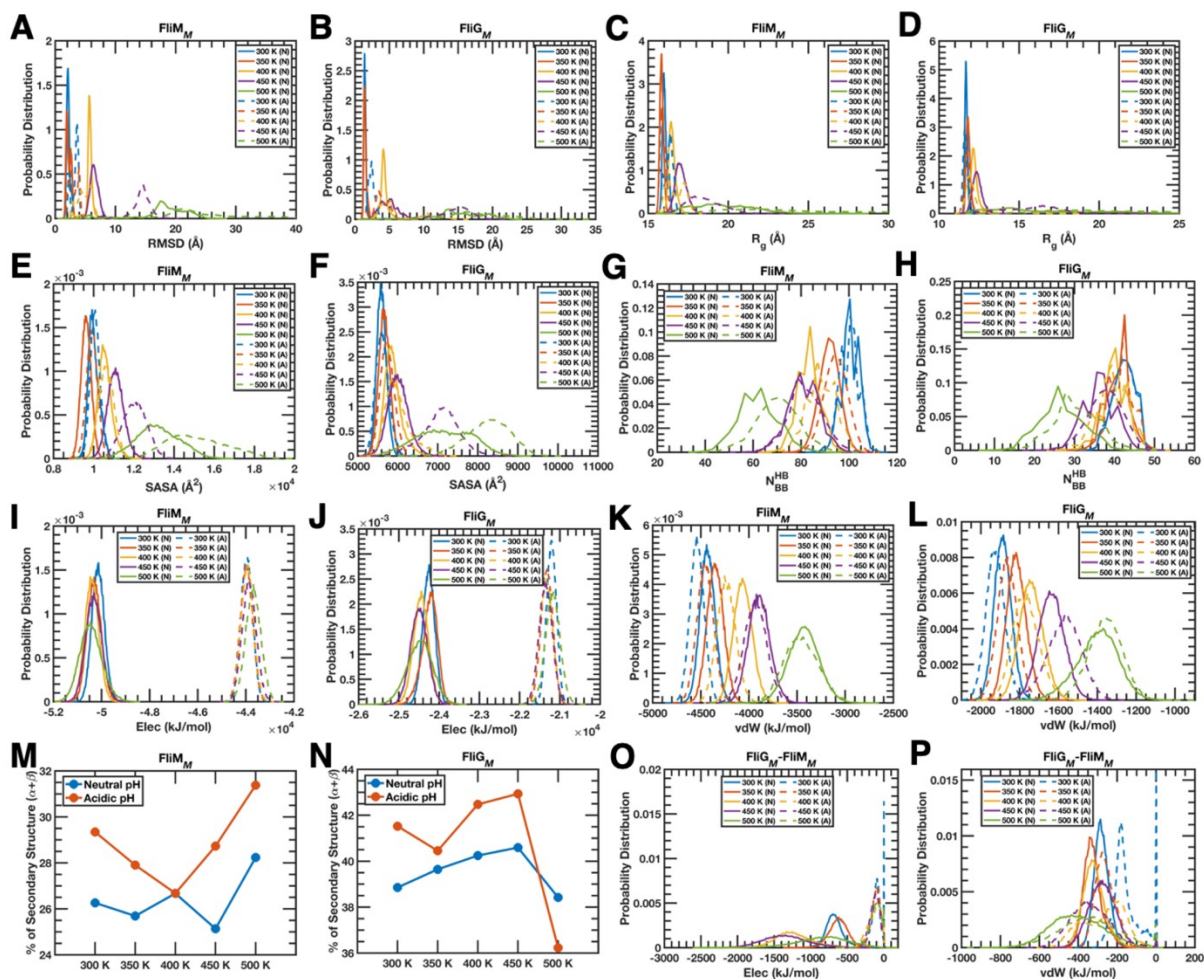


Figure S4. Modulation of structural and energetic features of the FliM_M and the FliG_M chains of the FliG_M-FliM_M complex due to changing temperature and pH conditions. (A-L) Normalized probability densities of the intra-protein properties – backbone RMSD (with respect the initial configuration) of (A) FliM_M protein and (B) FliG_M protein; backbone C_α-based R_g of (C) FliM_M protein and (D) FliG_M protein; global SASA of (E) FliM_M protein and (F) FliG_M protein; backbone hydrogen bonds of (G) FliM_M protein and (H) FliG_M protein; electrostatic interactions of (I) FliM_M protein and (J) FliG_M protein; and van der Waal's forces of (K) FliM_M protein and (L) FliG_M protein. Variation of the secondary structural percentage (α-helix+β-sheet) due to temperature and pH in (M) FliM_M protein and (N) FliG_M protein. Normalized probability densities of the modulated inter-chain features because of varying temperature and pH pertinent to the structural integrity of the complex – (O) functioning electrostatic interactions between two chains and (P) dispersion forces operating between two proteins.

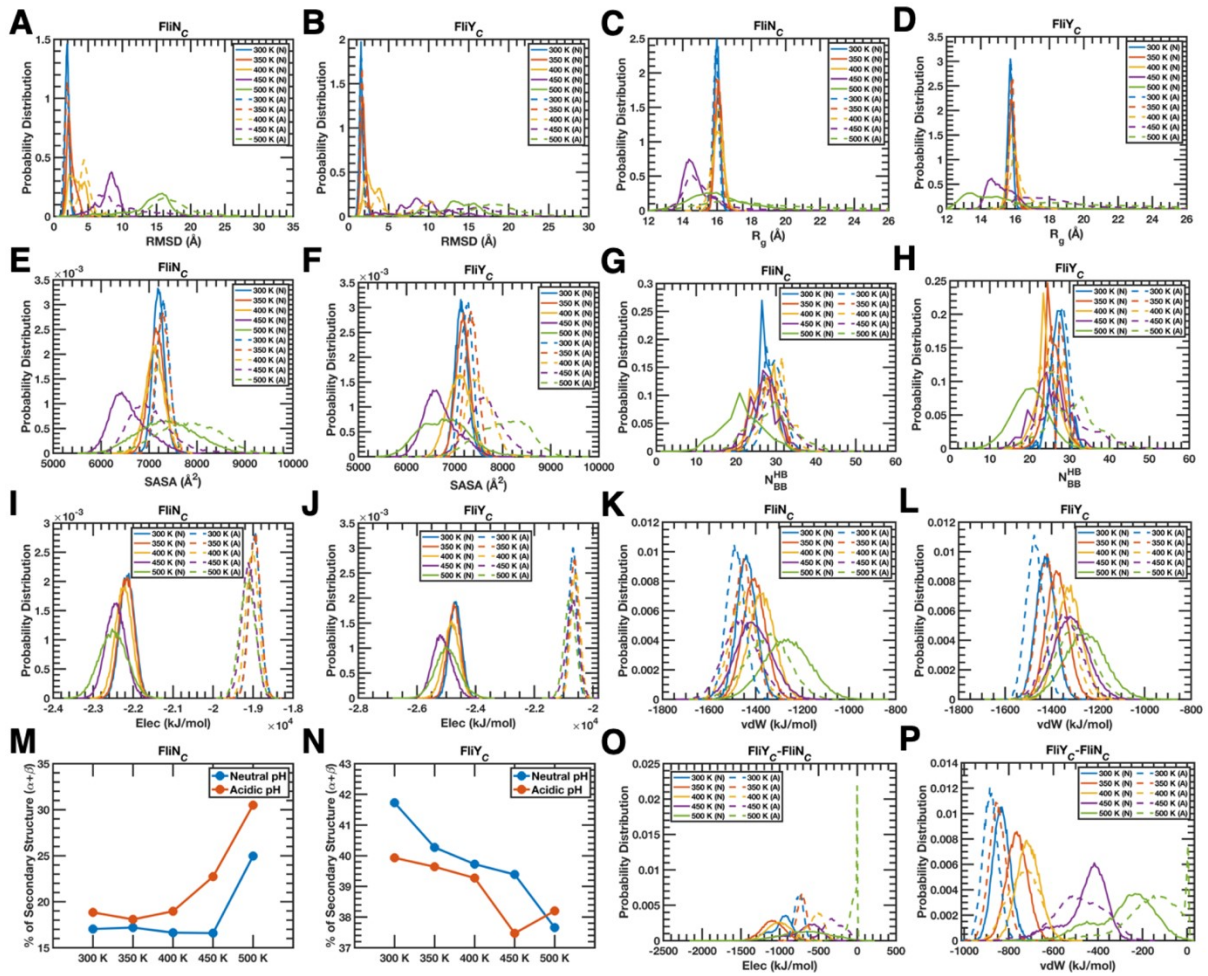


Figure S5. Change in structural and energetic properties of the FliY_C and the FliN_C chains of the FliY_C-FliN_C complex due to the altered environment caused by variable temperature and pH combinations. (A-L) Normalized probability densities of the intra-chain characteristics – backbone RMSD of (A) FliN_C chain and (B) FliY_C chain; backbone C_α-based R_g of (C) FliN_C chain and (D) FliY_C chain; global SASA of (E) FliN_C chain and (F) FliY_C chain; backbone hydrogen bonds of (G) FliN_C chain and (H) FliY_C chain; electrostatic forces of (I) FliN_C chain and (J) FliY_C chain; and van der Waal's interactions of (K) FliN_C chain and (L) FliY_C chain. Change in the secondary structural content (α-helix+β-sheet) as a result of variable temperature and pH in (M) FliN_C chain and (N) FliY_C chain. Normalized probability distributions of the altered inter-chain properties due to varying temperature and pH conditions – (O) operating electrostatic forces between two chains and (P) acting dispersion interactions operating between two proteins.

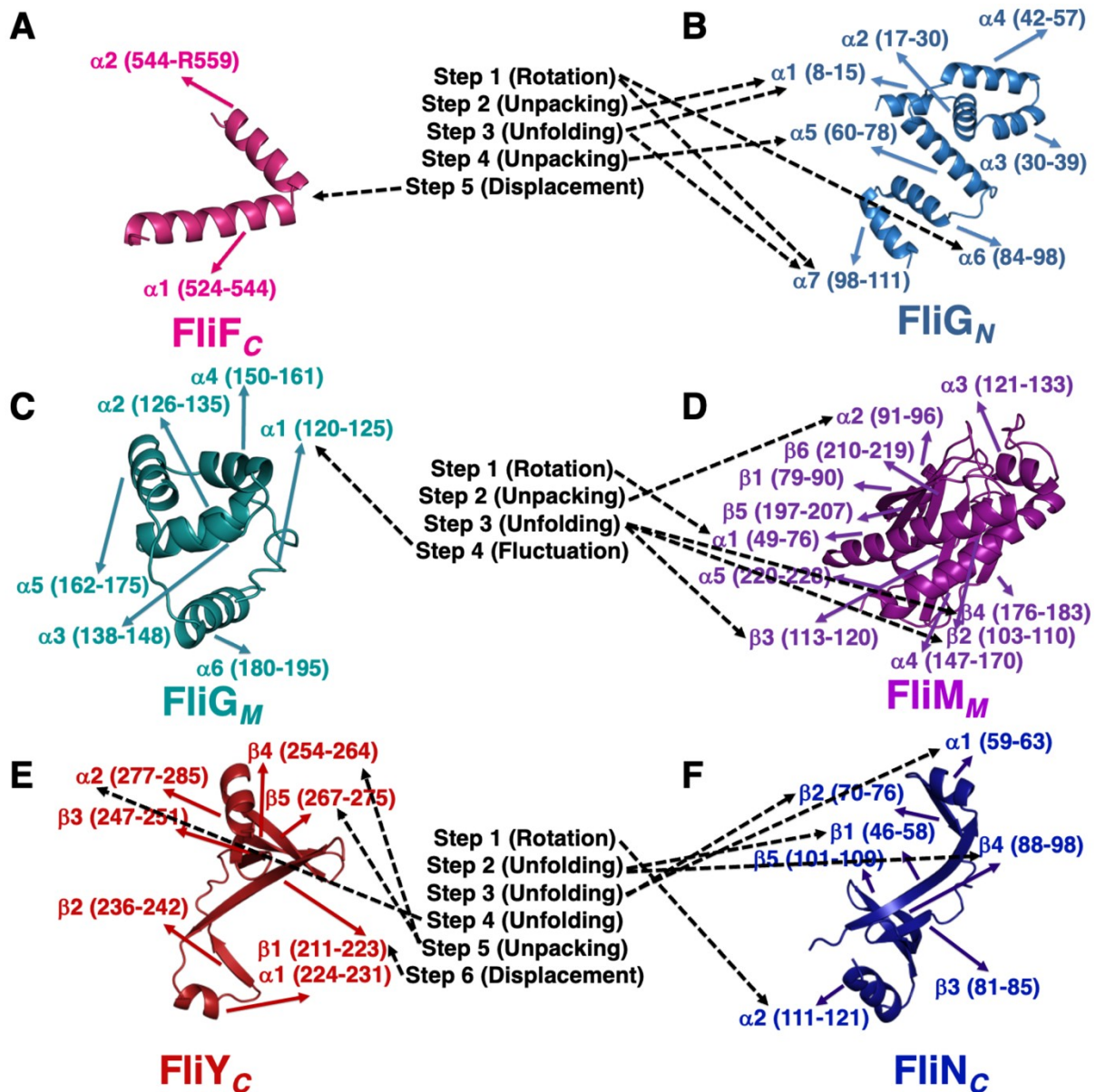


Figure S6. The unfolding mechanisms of the three complexes under thermal and/or pH-driven perturbation(s) highlighting the overall sequence of events in a chain-specific manner.

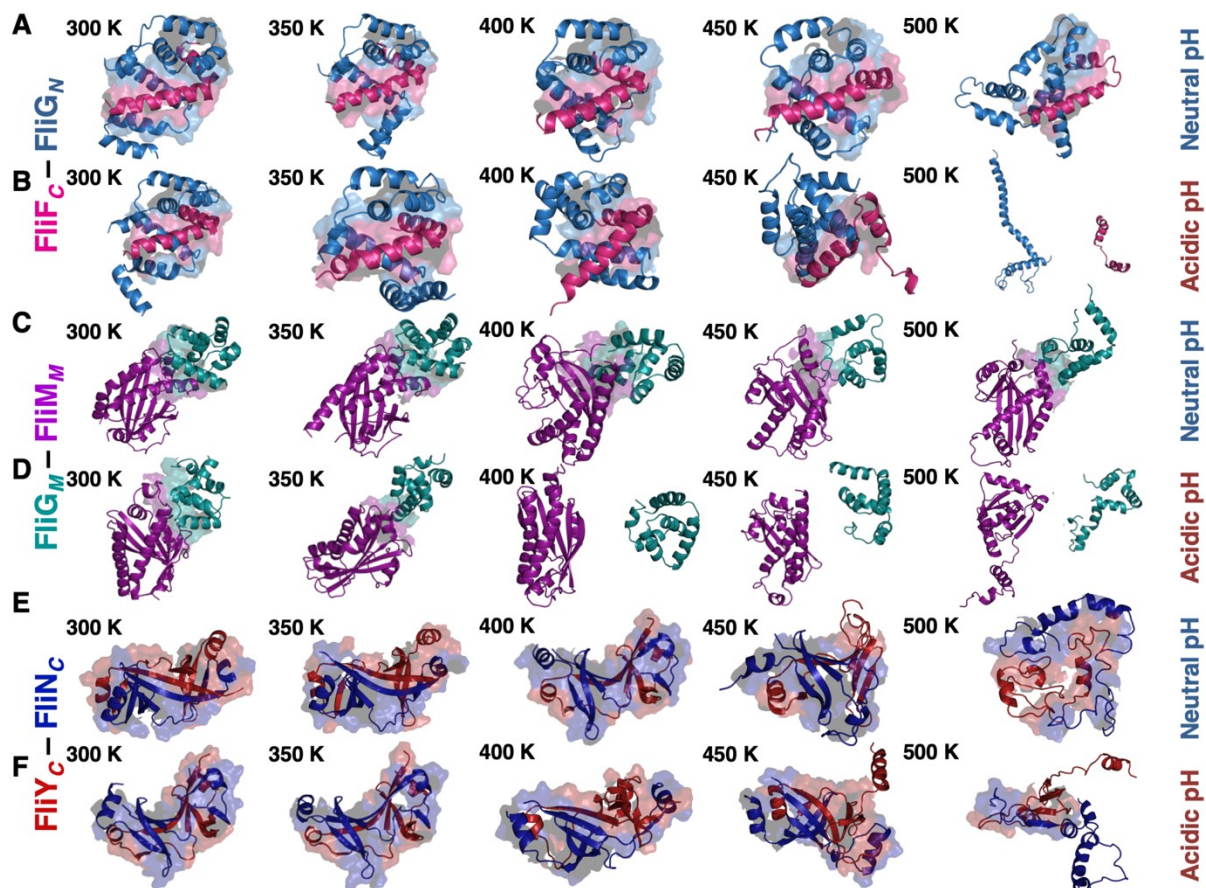


Figure S7. Modulation of interfacial interactions of the three complexes as a function of rising temperatures in two different pH conditions shown as surface since the residues involved in forming the interface are mentioned in terms of the secondary structural elements they belong to.

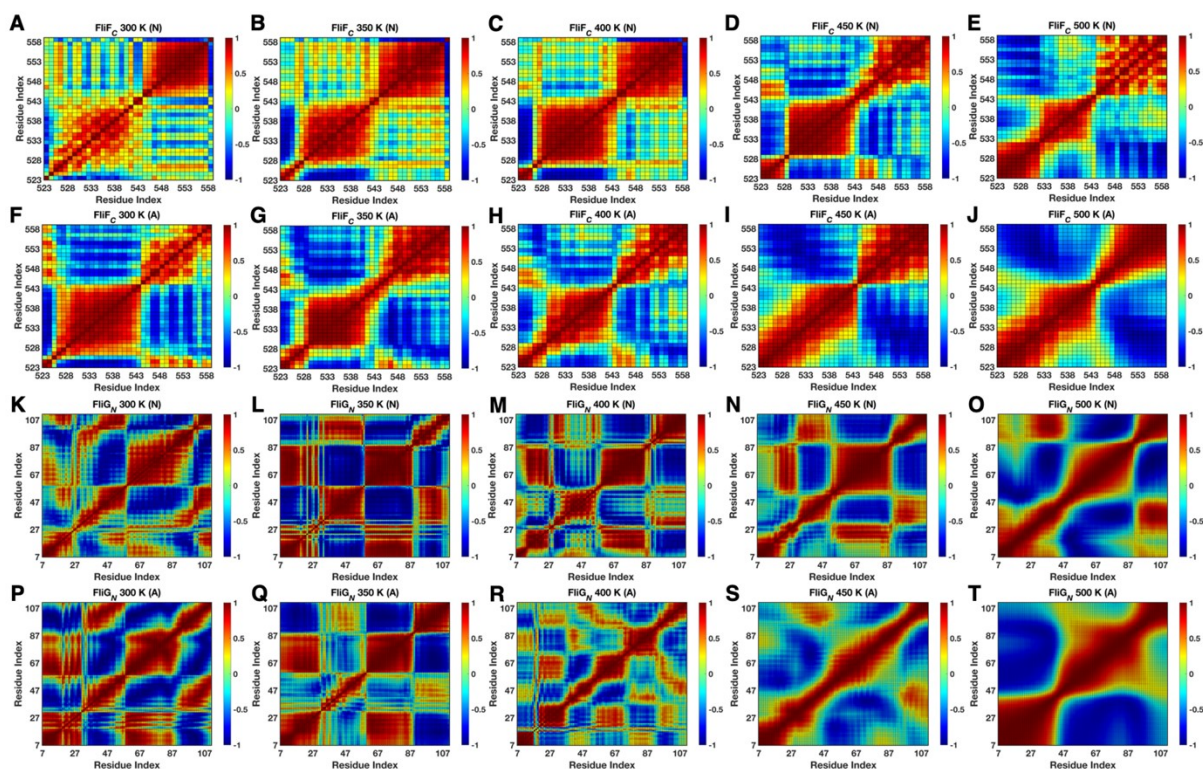


Figure S8. Intra-chain Dynamical Cross-Correlation Maps of the FliF_C and the FliG_N proteins of the FliF_C-FliG_N complex obtained from the unconstrained simulations at two different pH conditions and five different temperatures. The top of each panel describes the specific solution condition along with the identity of the protein chain.

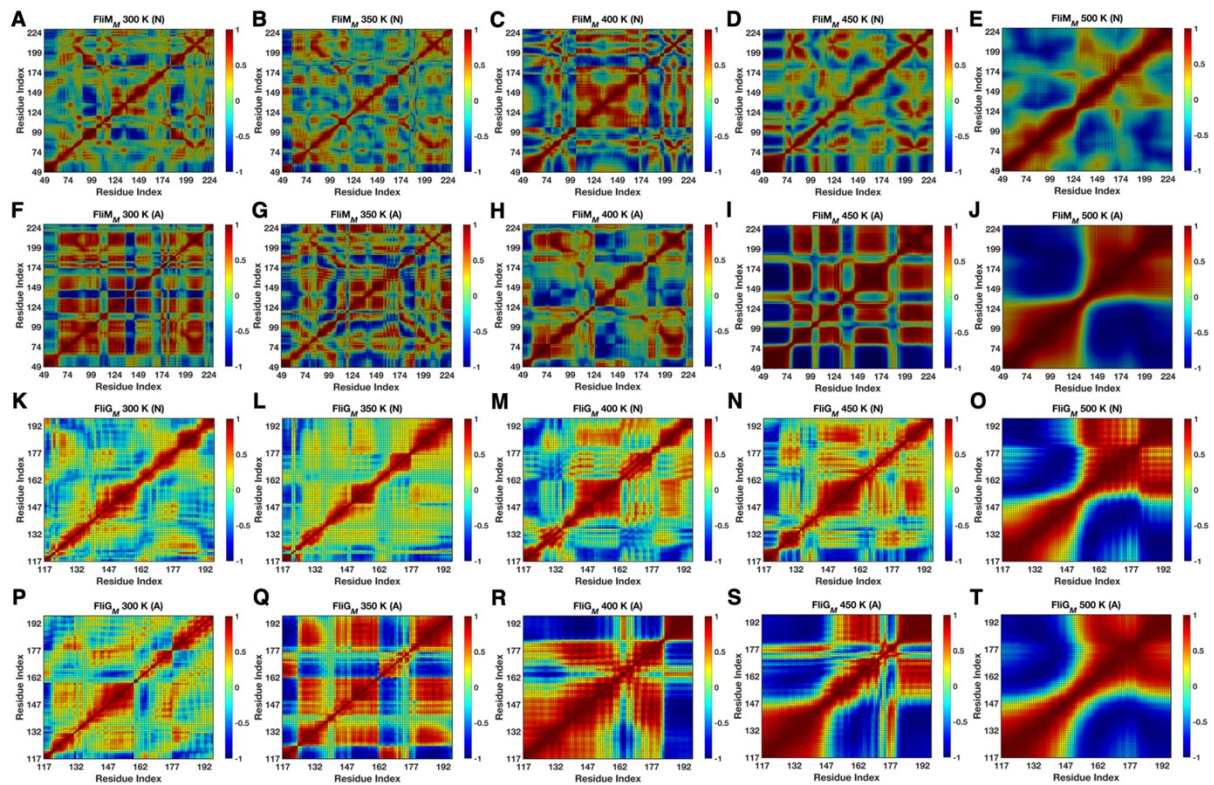


Figure S9. Intra-protein DCCMs of the FliG_M and the FliM_M sequences of the FliG_M-FliM_M complex. Each panel individually describes the identity of a specific protein sequence as well as the specific solution condition.

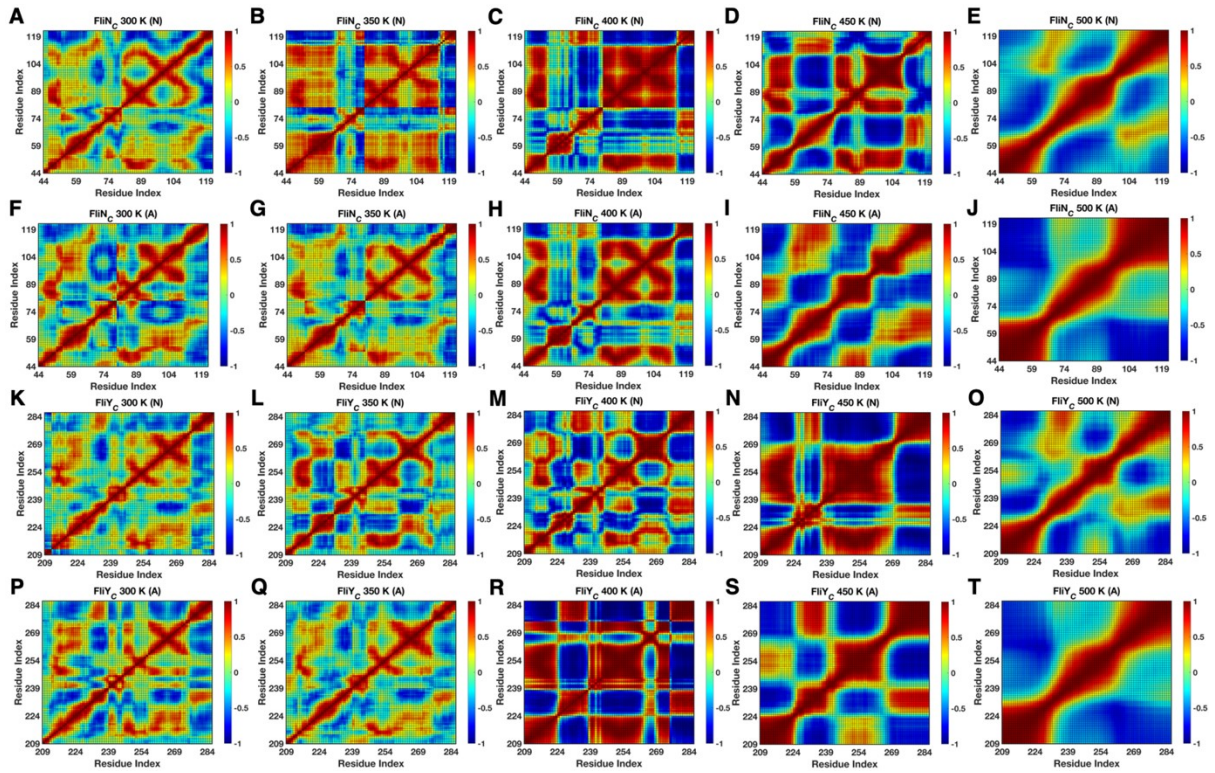


Figure S10. Intra-sequence DCCMs of the FliY_C chain and the FliN_C chain of the FliY_C-FliN_C complex at five different temperatures with the combination of neutral and acidic pH conditions. The top of each panel describes the identity of the specific chain, the temperature at which the complex was simulated, and the pH of the solution considered for the unconstrained simulation.

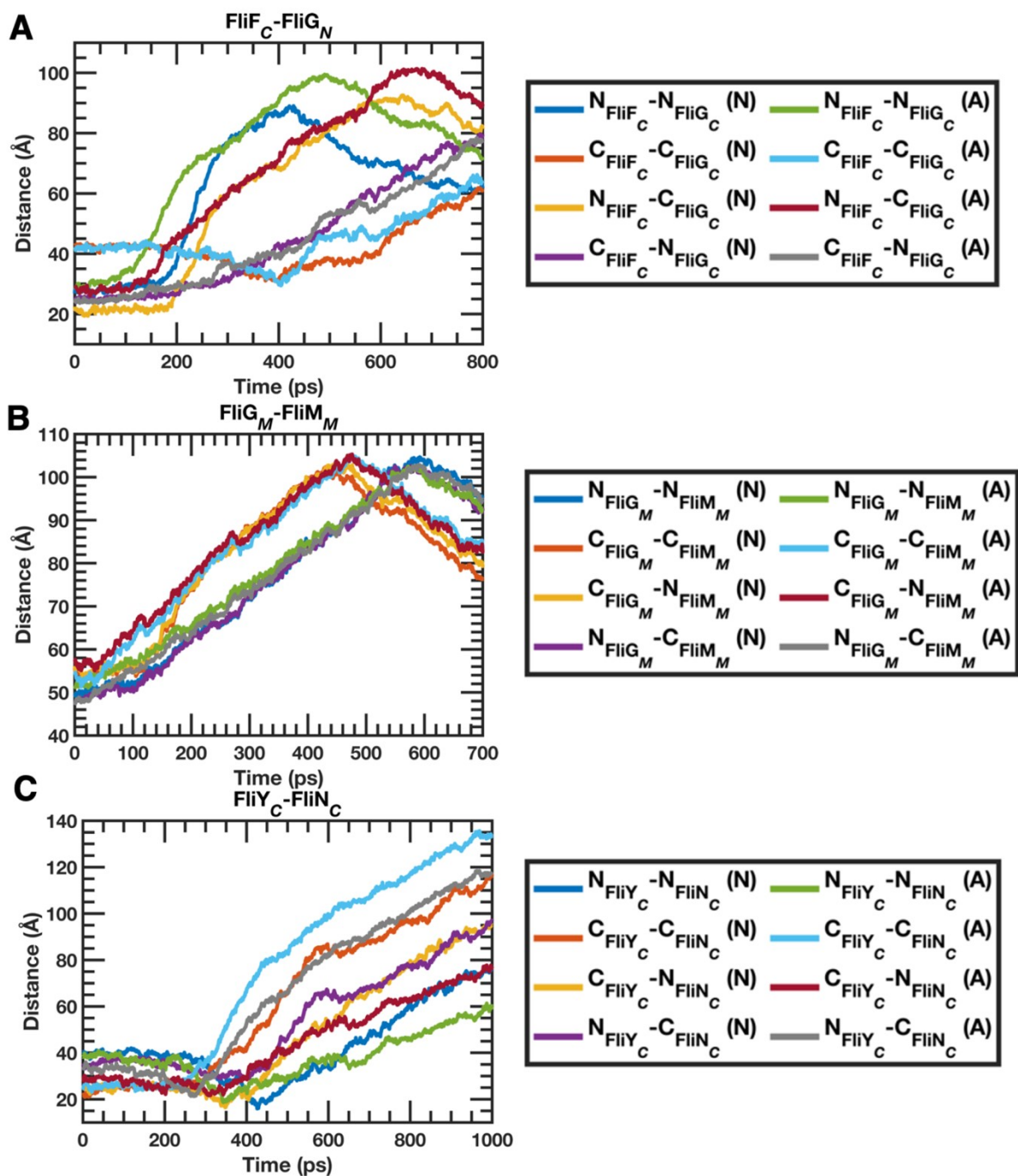


Figure S11. The time evolution of the distances between the two protein ends belonging to two different sequences, i.e., one between two N-termini, one between two C-termini, and two between two alternative termini – (A) the $FliF_C-FliG_N$ complex, (B) the $FliG_M-FliM_M$ complex, and (C) the $FliY_C-FliN_C$ complex.

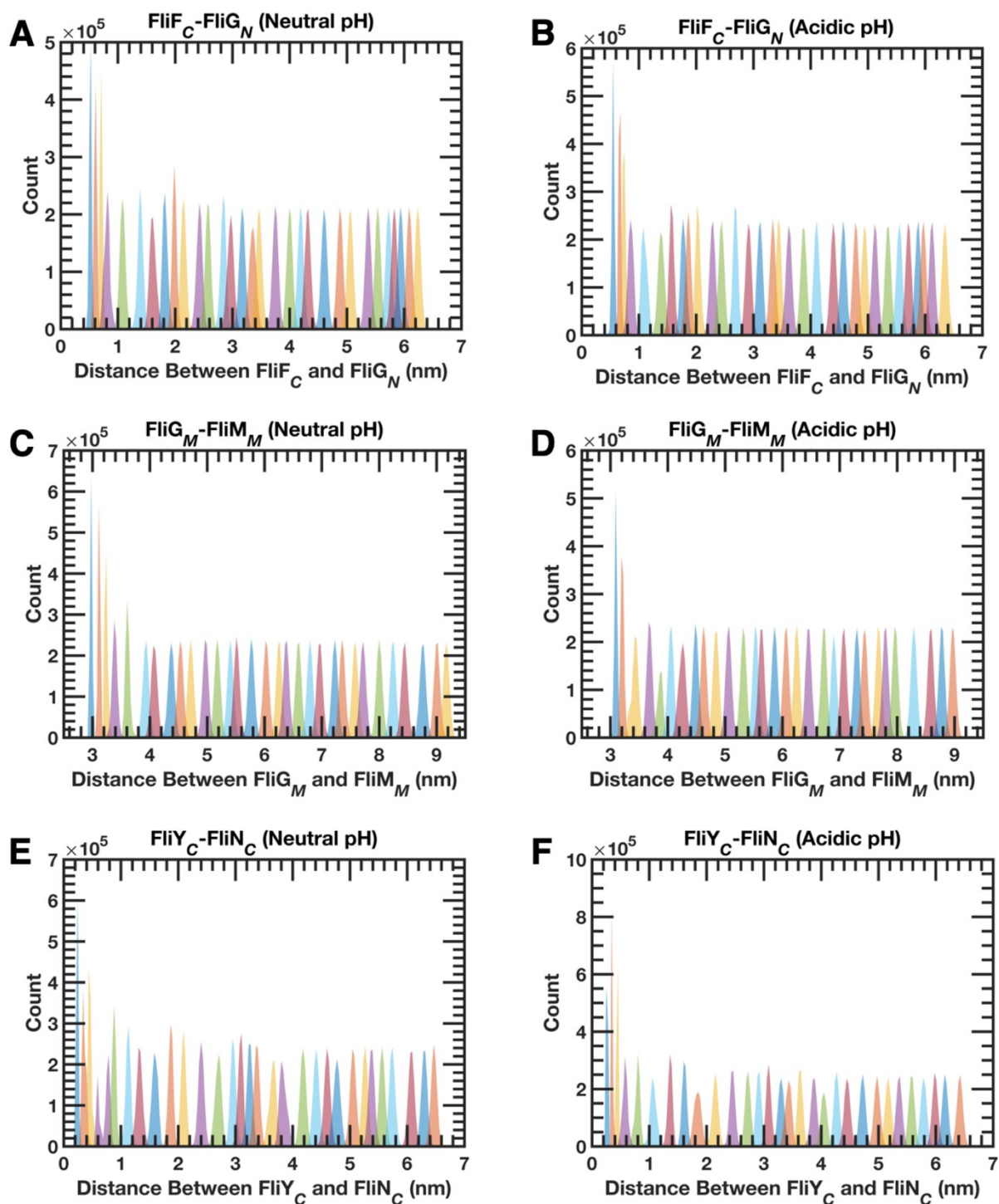


Figure S12. Overlap of potential energy distributions obtained from the individual umbrella windows for the three complexes in the two different pH conditions.